BCNNS synthesis using inductively coupled plasma: Band Gap control of graphene nanoflakes and boron nitride nanosheets

A. Alrebh[1] and J-L. Meunier[1]

[1]*Department of Chemical Engineering, McGill University, Montreal, Canada*

Abstract: Boron carbon nitride nanosheets (BCNNS) powders were synthesized in inductively coupled plasma. Ammonia borane was used as the boron and nitrogen source and methane as the carbon source. SEM/TEM images for BCNNS show two-dimensional graphene-like structures having lateral sizes of around 100-200 nm and ~5 nm in thickness. The structures show non-uniform layer stacking as well as dislocation-type defects. The band gap of BCNNS could be monotonically varied from 2.4 to 5.4 eV depending on the ratio of ammonia borane to methane injected in the reactor. Decreasing the methane flow rate results in the formation of segregated phases of C- and BN-rich material which exhibit variations in the band gap energy.

Keywords: BCNNS, graphene, BNNS, thermal plasma, Raman, band gap, optical emission.

1. Introduction

Boron carbon nitride nanosheets (BCNNS) are ternary materials composed of B, C, and N atoms of various compositions ($B_xC_yN_z$) having a 2-Dimensional (2D) hexagonal structure similar to graphene and boron nitride nanosheets. BCNNS have recently gained a particular attention especially due to their electrical properties and tuneable band gaps. This material has shown a promising performance in fuel cells, batteries, capacitors and other applications [1-3]. The presence of boron and nitrogen as heteroatoms in the carbon framework (i.e., graphene) plays a significant role in the improved performance and stability [4]. The addition of BN structures breaks the symmetry of the C−C structure and introduces a band-gab at the Fermi level [5]. This allows the control of the overall material's band gap to be between 0 and 5.6 eV, corresponding to the band gap of pure graphene and boron nitride nanosheets, respectively.

Several techniques have been developed to fabricate BCN nanomaterials such as catalytic, laser, microwave, plasma-enhanced CVD, pyrolysis, and molten salt method [6]. However, these methods and others lack the capability of producing free-standing BCNNS on a large scale, impeding the implementation of this material in various applications. Additionally, BCNNS made using these traditional methods tend to some extent to lack in regards to compositional and dimensional homogeneities.

Induction thermal plasma, on the other hand, has been shown by our group to be effective for graphene and boron nitride nanosheets synthesis on a large scale [7-10]. Thus, it is worthwhile to attempt free-standing BCNNS synthesis using this technique as a first step towards large scale production, and to gain understanding of the chemistry during the synthesis process. In this work ammonia borane (AB) and nitrogen (boron and nitrogen sources) and methane (carbon source) were decomposed in thermal induction plasma to produce BCNNS powders. The control of band gap energy was achieved through adjusting the ratio of methane to ammonia borane.

2. Experimental procedure

Radio frequency inductively coupled plasma (RF-ICP) operated at ~15 kW and 62 kPa was used to process ammonia borane, nitrogen and methane. The process conditions are listed in Table 1. Argon gas was used as the plasma-gas source. After the plasma jet formation, nitrogen was injected followed by methane. Ammonia borane was introduced immediately after the methane injection (Fig. 1). The conical geometry of the reaction chamber has shown in our past work on graphene that it enables a better control over the thermal history of the hot gases and precursors. This offers uniform thermal and species concentration gradients throughout the reaction/nucleation zone in the axial and radial directions [11].

The as-synthesized material (BCNNS) accumulated on the collecting plate. *In-situ* optical emission spectra (OES) were collected during the material synthesis at about 5 cm below the ICP torch nozzle. The OES is used to investigate the plasma chemistry during the material synthesis. BCNNS were characterized using various techniques including SEM, TEM, EDX, Raman and UV-Vis spectroscopies. The Tauc method was used to estimate the band gap energy of various BCNNS grades made with a specific ammonia borane feeding rate and various methane flow rates.

3. Results and discussion

The as-synthesized material contains mainly BCNNS and other by-products like boron and carbon particles as the SEM micrograph in Fig. 2a shows. BCNNS have large nanosheets (100-200 nm) that are very similar in morphology to graphene nanoflakes (GNF) and boron

nitride nanosheets (BNNS) obtained by the same method [7, 9].

Table 1. Conditions of BCNNS synthesis.

Carrier gas	Argon (Ar): 1 slpm
Central gas	Ar: 15 slpm
Sheath gas	Ar: 40 slpm Nitrogen (N_2): 10 slpm
Solid feedstock	Ammonia borane (AB): 100 mg/min (0 mg/ming for GNF synthesis)
Gas feedstock	Methane (CH_4): 0 - 500 sccm (increment of 100 sccm to synthesize GNF, BCNNS-1, -2, -3, -4, and -5, respectively)
Plasma power	14.5 kW
Pressure	62 kPa

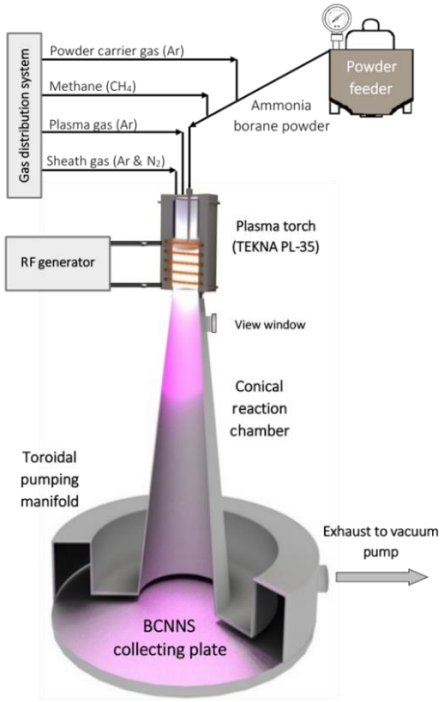

Figure 1. Schematics of RF-ICP setup.

A typical TEM image for the material is shown in Fig. 2b. The sheet thickness is 1-4 nm containing 3-10 layers with an interlayer spacing of ~0.37 nm which is slightly larger than those observed in GNF and BNNS. The layer stacking is rippled and not uniform (see insert of Fig. 2b) as compared to GNF and BNNS. The arrows in Fig. 2b are pointing to dislocation-type defects that may be responsible for the rippling effect. We speculate that these defects result from B−N segregating from C−C, forming B−N islands in the C lattice. The deviation of the interlayer spacing from the theoretical value is perhaps due to the variations in strengths of the Van der Waal weak forces in-between the A-B stacked layers.

Fig. 2c-f show a HAADF image and its associated elemental distribution of boron, carbon and nitrogen, respectively, obtained by EDX. The three elements are dispersed homogeneously and evenly throughout the sheet. This indeed demonstrates that ternary BCN nanosheets were effectively formed by the thermal plasma method.

Graphitization of BCNNS was investigated using Raman spectroscopy. Fig. 3a,b show normalized Raman scattering spectra in the range of 1000-1800 cm^{-1} for two grades of BCNNS made with high and low methane flow rates, respectively, at a specific feeding rate of ammonia borane. Lorentzian function deconvolution was applied to these spectra to reveal bands that are typical of graphitized BCN materials: D (1340 cm^{-1}), and G (1570 cm^{-1}) bands and their shoulders D", D_3 and D'. The G band arises from C−C bond stretching E_{2g} mode in C-based graphitic materials, while the D band is induced by A_{1g} breathing mode due the disorderness in the crystal. Thus, the intensity ratio of D to G (I_D/I_G) has been used as a measure for the level of disorderness in graphene [12]. I_D/I_G for GNF (Raman spectrum not shown), BCNNS-1, and BCNNS-2 were found to be 0.48, 0.99, and 1.48. The increase in I_D/I_G is associated with the increase in disorderness and defects as the AB:CH_4 ratio in the feedstock increases.

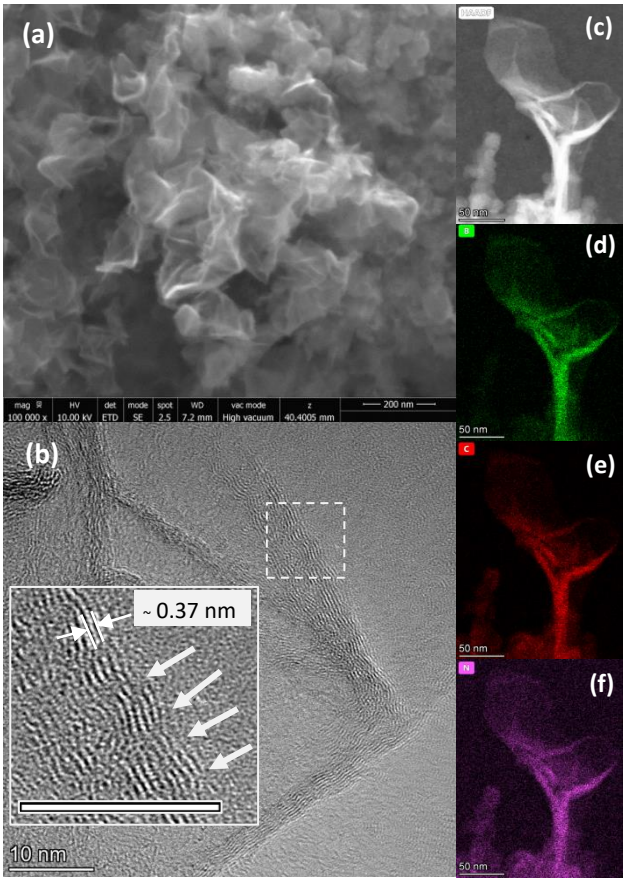

Figure 2. a) SEM and b) TEM of BCNNS, c) HAADF image and EDX elemental mapping for d) B, e) C, and f) N.

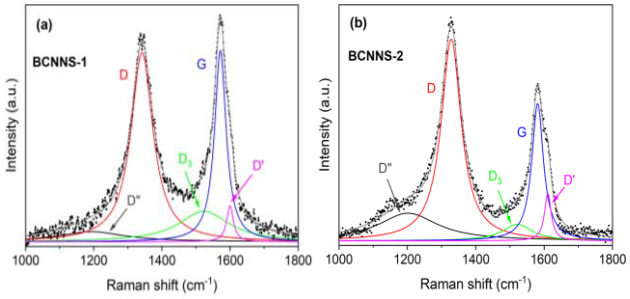

Figure 3. Raman spectra and their Lorentzian function deconvolution for BCNNS made with a) high and b) low methane flow rates, BCNNS-1 and -2, respectively. The deconvolution reveals D", D, D_3, G and D' peaks.

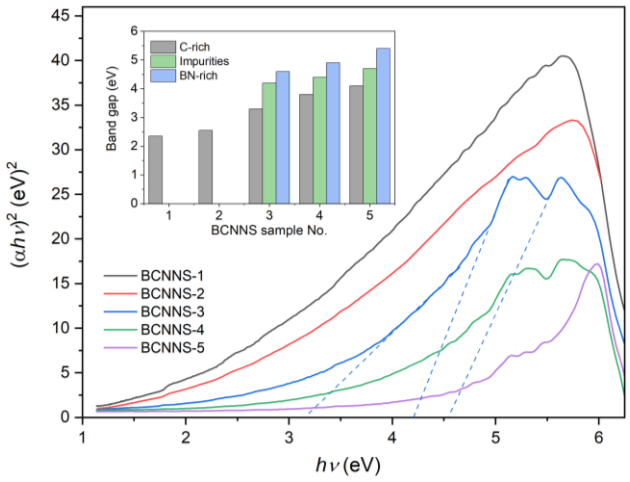

Figure 4. Tauc plots of five BCNNS samples made of a specific feeding rate of ammonia borane and decreasing flow rates of methane (black highest, purple lowest). Inset: Band gap values of the five BCNNS samples. The estimation of these values were done by extrapolating the curves as demonstrated by the blue curve.

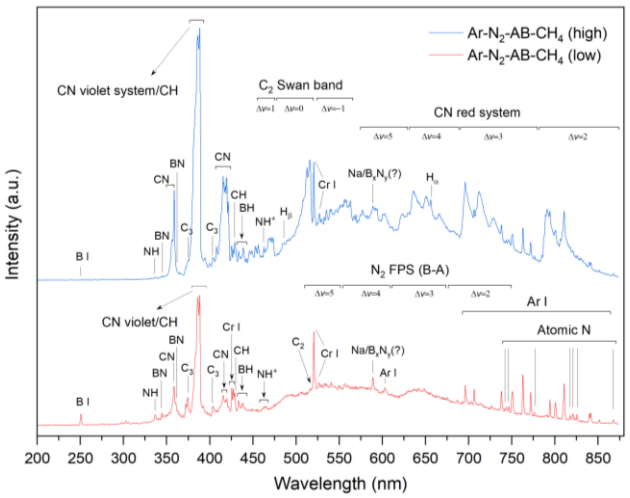

Figure 5. OES for Ar-N_2-AB-CH_4 at high (blue) and low (red) methane flow rates associated with the synthesis of BCNNNS-1 and -5, respectively.

Other defect-induced bands are D" (shoulder to the left of D) and D' (shoulder to the right of G). D" originates from double-resonant scattering of longitudinal acoustic phonons with defects. It is normally found in bi- and few-layered graphene and carbon nanotubes [13]. D', on the other hand, has been attributed to the disorder-induced phonon mode due to crystal defects. The intensity ratios $I_{D"}/I_G$ and $I_{D'}/I_G$ are seen to increase as AB:CH_4 increases following this sequence: GNF < BCNNS-1 < BCNNS-2. D^3, located between the D and G peaks, is related to the presence of amorphous carbon, and also relates to the presence of 5- and 8-ring defects [12, 14, 15]. These findings may suggest that B and N are embedded in the C−C network as 'defects', and when the AB:CH_4 ratio increases, the number of these defects increases accordingly.

The band gap energy of five different BCNNS samples were estimated using the Tauc method. These samples were prepared using a specific feeding rate of ammonia borane and a decreasing flow rate of methane (increasing ratio of AB:CH_4) at the same experimental conditions. As Fig. 4 and its inset show, the band gap energy increases monotonically (grey bars) with the decrease in CH_4. At low CH_4, a phase separation in the as-synthesized material occurs. These phases are a C-rich phase, a BN-rich phase, and impurities. C−C is dominant in C-rich and the defects are B−N, while the opposite is true for the BN-rich phase. The impurity fraction, according to TEM images (not shown here), represents carbon particles coated with BN in core-and-shell structures. The band gap energy of these three phases are seen to increase as the AB:CH_4 ratio increases (inset of Fig. 4).

Optical emission spectroscopy was used to study the chemistry of BCNNS formation reaction during the decompsotion process of AB, N_2 and CH_4. Two cases were selected in which the AB feeding rate was the same while the CH_4 flow rate was low in one case and high in another. Fig. 5 shows the OES spectra of these two cases (red and blue curves represent low and high CH_4 flow rates, respectively).

The most obvious feature is the absence of the C_2 Swan band $A\,^3\Pi_g - X\,^3\Pi_u$ (466-563 nm for Δv=1, 0 and –1) and CN red system $A\,^2\Pi - X\,^2\Sigma$ (544-806 nm for Δv=5, 4, 3 and 2) in the low CH_4 case, while both appear when CH_4 flow rate is high. CN violet system $B\,^2\Sigma - A\,^2\Pi$ (358-418 nm for Δv=1, 0 and –1), C_3 Swings band $A\,^1\Pi_u - X\,^1\Sigma_g$ (~405 and 374 nm), CH $A\,^2\Delta - X\,^2\Pi$ (388.9 and 431.4 nm), and BH $^1\Pi - {}^1\Sigma$ (433-443 nm for Δv=0) are present in both cases, albeit being more pronounced in the case of high CH_4 flow rate, which explains the formation of C-dominant BCNNS. B I (~250 nm), BN $^3\Pi \rightarrow {}^3\Pi$ (343-346 nm and 359-365 nm for Δv=1 and 0, respectively), NH $A\,^3\Pi - X\,^3\Sigma$ (305 nm and 336-337 nm for Δv=1 and 0, respectively), and N_2 FPS $B\,^3\Pi_g - A\,^3\Sigma^+_u$ (503-750 nm for Δv=6, 5, 4, 3, and 2) appear stronger in the low CH_4 case. These species appear stronger in the low CH_4 case given that the majority of the reaction results in the formation of BN-dominant BCNNS.

4. Conclusion

Boron carbon nitride nanosheets (BCNNS) powders were effectively synthsized in inductively coupled plasma using ammonia borane (AB), nitrogen and methane (CH_4). High resolution electron microscopy showed that the morphology of the material resembles that of graphene nanoflakes and boron nitride nanosheets, although deviated from their interlayer spacing and layer stacking uniformity. Raman spectroscopy showed an increase in the defects-induced peaks due to inclusion of B, N and BN in the C matrix, and the peak intensities were directly proprtional to the BN content. Control of the band gap energy was seen to be possible and achieved through adjusting the AB:CH_4 ratios in the feedstock. This work represents a first and important step towards free-standing BCNNS synthesis and the control of their band gap.

5. References

[1] K. Moses, et al., *Chemistry–An Asian Journal* **9**, 838 (2014).

[2] J. Zhang, et al., *The Journal of Physical Chemistry C* **125**, 4946 (2021).

[3] H. Jiang, et al., *ACS Applied Materials & Interfaces* **12**, 47425 (2020).

[4] C. L. Muhich, et al., *The Journal of Physical Chemistry C* **117**, 10523 (2013).

[5] A. Bafekry and C. Stampfl, *Physical Review B* **102**, 195411 (2020).

[6] S. Angizi, et al., *ECS Journal of Solid State Science and Technology* **9** (2020).

[7] R. Pristavita, et al., *Plasma Chemistry and Plasma Processing* **30**, 267 (2010).

[8] J.-L. Meunier, et al., *in* "21st International Symposium on Plasma Chemistry", 2013.

[9] A. Alrebh and J.-L. Meunier, *2D Materials* **8**, 045018 (2021).

[10] A. Alrebh and J.-L. Meunier, *Plasma Chemistry and Plasma Processing* (2022).

[11] J.-L. Meunier, et al., *Plasma Chemistry and Plasma Processing* **34**, 505 (2014).

[12] R. Poyato, et al., *Materials* **13**, 2656 (2020).

[13] F. Herziger, et al., *Physical Review B* **90**, 245431 (2014).

[14] K. N. Kudin, et al., *Nano letters* **8**, 36 (2008).

[15] S. Claramunt, et al., *The Journal of Physical Chemistry C* **119**, 10123 (2015).